Journal of ELECTRONIC MATERIALS, Vol. 46, No. 1, 2017
DOI: 10.1007/s11664-016-4836-3
© 2016 The Minerals, Metals & Materials Society

Structural and Thermoelectronic Properties of Chalcopyrite $MgSiX_2$ (X = P, As, Sb)

B. KOCAK,[1] Y.O. CIFTCI,[1,4] and G. SURUCU[2,3]

1.—Department of Physics, Gazi University, Teknikokullar, 06500 Ankara, Turkey. 2.—Department of Electrics and Energy, Ahi Evran University, 40100 Kirsehir, Turkey. 3.—Photonics Application and Research Center, Gazi University, 06500 Ankara, Turkey. 4.—e-mail: yasemin@gazi.edu.tr

We have explored the structural, electronic, optical, and mechanical properties of the magnesium-based chalcopyrites $MgSiP_2$, $MgSiAs_2$, and $MgSiSb_2$ using density functional theory with five different generalized gradient approximation (GGA) functionals: Perdew–Wang (1991), Perdew–Burke–Ernzerhof, revised Perdew–Burke–Ernzerhof, modified Perdew–Burke–Ernzerhof for solids, and Armiento–Mattson (2005) as well as the local density approximation. Change of the constituent element from P to Sb significantly affected the lattice constants, elastic constants, and thermal and dielectric properties. Our theoretically computed results are in reasonable agreement with experiments and other theoretical calculations. The electronic band structure results imply that all three considered compounds are semiconductors. $MgSiP_2$ has the highest value of elastic constants, and bulk and shear moduli compared with the other two binary chalcopyrites. Furthermore, the optical response in terms of the dielectric functions, optical reflectivity, refractive index, extinction coefficient, and electron energy loss of the compounds were also investigated in the energy range from 0 eV to 15 eV. The calculated optical results reveal optical polarization anisotropy for all three compounds, making them useful for optoelectronic device applications. Moreover, specific focus is also given to quantify the dependence of various thermal properties on finite pressure/temperature within the quasiharmonic approximation.

Key words: Chalcopyrites, semiconductor, thermal properties, optical properties

INTRODUCTION

The family of chalcopyrite semiconductor materials with I–III–VI_2 and II–IV–V_2 structure type is unique in that they are natural prime candidates for use in spintronic, optoelectronic, nonlinear optical, and photovoltaic applications, due to their wide variety of interesting physical properties.[1–10]

The Mg–IV–V_2 (IV = Si, Ge, Sn; V = P, As, Sb) chalcopyrites span a range of structural, optical, and electronic properties, making them ideal for integration into III–V-compound-based optoelectronic devices and applications.[1–21] Previous theoretical studies have determined various structural, elastic, and optical properties, including detailed study of the electronic band structure of $MgSiP_2$, $MgSiAs_2$, and $MgSiSb_2$; For instance, Jaffe et al.[5] first determined the structural and electronic band structure of various II–IV–V_2-type compounds, including the title compounds, using self-consistent band-structure methods. The linear optical properties of II–IV–V_2 compounds (II = Mg, Zn, Cd; IV = Si, Ge; V = P, As) were investigated by Chiker et al.[15] using the full potential linearized augmented plane wave (FP-LAPW) method. Shaposhnikov et al.[18] obtained the structural, electronic, and optical properties of II–IV–V_2 (II = Be, Mg, Zn, Cd; IV = Si, Ge, Sn; V = P, As) chalcopyrite-type ternaries with the aid of the

(Received March 21, 2016; accepted July 28, 2016; published online August 18, 2016)

Table I. Equilibrium lattice constants (a and c in Å), $c/2a$ ratio, bulk modulus (B in GPa), and pressure derivative of bulk modulus (dB/dP) for $MgSiX_2$ (X = P, As, Sb) calculated using various exchange–correlation functionals at 0 GPa and 0 K, compared with earlier studies

Compound	Reference	a (Å)	c (Å)	$c/2a$	u	B (GPa)	dB/dP
$MgSiP_2$	Present (LDA-CA)	5.680	10.020	0.882	0.2915	81.395	4.106
	Present (GGA-PW91)	5.747	10.242	0.891	0.292	73.018	4.140
	Present (GGA-PBE)	5.748	10.235	0.890	0.292	72.988	4.139
	Present (GGA-RPBE)	5.780	10.319	0.893	0.293	69.505	4.160
	Present (GGA-PBEsol)	5.7396	10.054	0.876	0.293	77.341	4.095
	Present (GGA-AM05)	5.7395	10.084	0.878	0.293	76.159	4.108
	Exp.[30]	5.718	10.109	0.885	0.292		
	Theory[4]	5.700	9.804	0.860	0.288		
	Theory (LDA)[9]	5.640	10.942	0.970	0.300	75.000	4.300
	Theory (GGA-PBE)[20]	5.852	10.422	0.891	0.297		
	Theory (GGA)[18]	5.733	10.242	0.893	0.292		
	Theory (LDA)[21]	5.694	10.124	0.889	0.292		
	Theory (GGA-PBE)[11]	5.440	9.683	0.890	0.292	73.920	3.820
$MgSiAs_2$	Present (LDA-CA)	5.874	10.531	0.896	0.285	66.455	4.178
	Present (GGA-PW91)	5.966	10.802	0.905	0.285	58.417	4.230
	Present (GGA-PBE)	5.969	10.795	0.904	0.285	58.230	4.227
	Present (GGA-RPBE)	6.008	10.899	0.907	0.286	54.744	4.254
	Present (GGA-PBEsol)	5.940	10.590	0.891	0.286	63.109	4.190
	Present (GGA-AM05)	5.941	10.623	0.894	0.287	61.757	4.204
	Theory[5]	5.804	10.853	0.935	0.284		
	Theory (GGA)[18]	5.954	10.800	0.907	0.286		
	Theory (LDA)[21]	5.885	10.569	0.898	0.285		
	Theory (GGA-PBE)[20]	5.956	10.614	0.891	0.290		
$MgSiSb_2$	Present (LDA-CA)	6.323	11.708	0.926	0.278	49.574	4.286
	Present (GGA-PW91)	6.433	11.946	0.929	0.279	43.05	4.303
	Present (GGA-PBE)	6.434	11.938	0.928	0.279	42.576	4.472
	Present (GGA-RPBE)	6.484	12.060	0.930	0.280	39.805	4.327
	Present (GGA-PBEsol)	6.387	11.729	0.918	0.280	46.943	4.265
	Present (GGA-AM05)	6.394	11.775	0.921	0.281	45.443	4.286
	Theory[5]	6.221	11.683	0.939	0.281		
	Theory (GGA-PBE)[20]	6.348	11.604	0.914	0.287		

modified Becke–Johnson (mBJ) exchange–correlation potential and GW approximation. Ouahrani[11] studied the structure, phase transition (from chalcopyrite to NaCl), electron localization function, and local compressibility of $XSiP_2$ (X = Be, Mg, Cd, Zn, Hg) under pressure using first-principles calculations with Elk and WIEN2k, a full potential linear augmented plane wave (FP-LAPW) code, within the Perdew–Burke–Ernzerhof (PBE) generalized gradient approximation (GGA). Subsequently, the calculated dynamical and anisotropic behaviors of the same compounds were newly reported by Ouahrani et al.[12]

Due to the technological importance of these compounds, it appears necessary to comprehend the behavior of their thermal properties at high temperature or pressure, which is the focus of this work. Although a very similar approach was used by Ullah et al.[19] to explain the electronic and optical properties of $MgYZ_2$ (Y = Si, Ge; Z = N, P), our calculations differ in the use of various exchange–correlation functionals. They also used the full potential linearized augmented plane wave plus local orbital (FP-LAPW) method based on DFT, as implemented in the WIEN2K package, performing the Engel–Vosko (EV) GGA scheme. They deduced that the bandgap and reflectivity calculated for their compounds were high in the visible and ultraviolet regions of the energy spectrum, making them useful for photonic, optoelectronic, and optical applications. Recently, in another similar study, Shi et al.[20] carried out calculations for $BeSiV_2$ and $MgSiV_2$ (V = P, As, Sb) in chalcopyrite phase to predict their elastic properties, phonon dispersion relations, phonon density of states, infrared absorption spectra, and Raman scattering spectra within the PBE GGA as implemented in the Cambridge Serial Total Energy Package (CASTEP) code.

Despite these various theoretical first-principles studies, there remains considerable uncertainty regarding the electronic, optical, and mechanical properties, especially for the compound $MgSiSb_2$. The main aim of this study is to predict the ground-state, elastic, electronic, optical, and thermal properties using density functional theory (DFT). To provide significant information for application and design of these compounds, we attempt to use several exchange–correlation functionals,[22–27] as

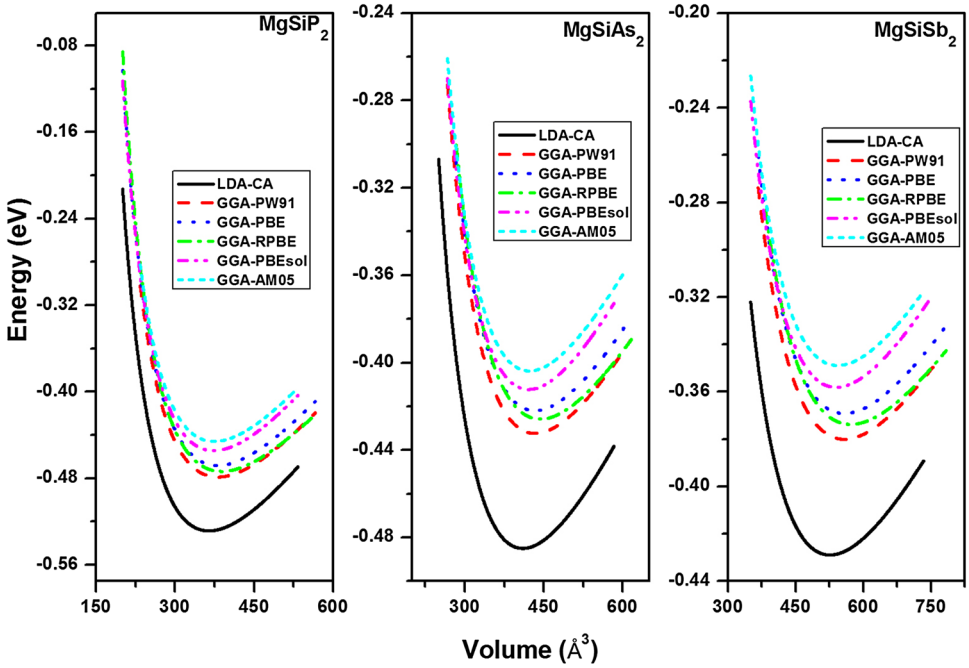

Fig. 1. Total energy versus volume calculated using several exchange–correlation functionals for $MgSiX_2$ (X = P, As, Sb) compounds in chalcopyrite phase.

mentioned above. The main results were obtained using the projector augmented-wave method[28] as implemented in the Vienna *ab initio* Simulation Package (VASP).[29] After careful tests, the kinetic-energy cutoff for the plane-wave expansion was taken as 500 eV and the Brillouin zone was sampled using a special $9 \times 9 \times 5$ **k**-point grid, except for the electronic density of states and charge density, because such calculations require a dense mesh, hence the Brillouin zone was sampled using a $17 \times 17 \times 10$ **k**-point grid. The convergence criterion for structural optimization was 10^{-7} eV.

RESULTS AND DISCUSSION

Structural Properties

Whereas $MgSiP_2$ crystallizes in a body-centered tetragonal phase (space group no. 122, $I\bar{4}2d$, $D2_d$), $MgSiAs_2$ and $MgSiSb_2$ have not yet been synthesized. Throughout this study, we optimized all the considered compounds in space group $D2_d$ with Mg atoms at (0 0 0), Si atoms at (0.0 0.0 0.5), and X (X = P, As, Sb) atoms at (u 0.25 0.125). As is well known, the body-centered tetragonal structure can be simply defined by three lattice parameters: a and c, and an internal parameter u. Since crystal structure optimization plays a fundamental role in determining the electronic and thermal properties of a material, we selected several exchange–correlation functionals to increase the reliability of our results. The calculations of the structural properties of $MgSiX_2$ (X = P, As, Sb) were performed with full structure relaxation for all free internal atomic positions. A comparison between the calculated and experimental values of all of the relevant equilibrium unit-cell parameters, bulk modulus (B), and pressure derivative of bulk modulus (dB/dP), as obtained by fitting the Murnaghan equation of state (EOS), for these compounds is presented in Table I. The cell volume increased from the P to Sb compound, as expected. It is well known that the ideal crystal has tetragonal distortion with $n = 1$ (where $n = c/2a$) and $u = 0.25$ in the body-centered tetragonal phase. In all the $MgSiX_2$ (X = P, As, Sb) compounds, both the tetragonal distortion ratio ($c/2a$) and internal parameter (u) are nonideal due to deviation from the ideal crystal structure.

The total energy computed as a function of the unit-cell volume for $MgSiX_2$ (X = P, As, Sb) is presented in Fig. 1 for several exchange–correlation functionals. Whereas the lattice constant a of $MgSiP_2$ obtained from the current calculations with the LDA is nearly 0.7% smaller (↓) than the experimental value (a_{exp} = 5.718 Å),[30] the values obtained with the PW91, PBE, RPBE, PBEsol, and AM05 GGA functionals are higher (↑) by 0.5%, 0.53%, 1.08%, 0.378%, and 0.376%, respectively, compared with the experimental result. For $MgSiP_2$, the lattice constant c shows a small error of 0.88% (↓), 1.32% (↑), 1.25% (↑), 2.08% (↑), 0.54% (↓), and 0.25% (↓) for the LDA, PW91, PBE, RPBE, PBEsol, and AM05 calculations, respectively, as compared with the experimental result (c_{exp} = 10.109 Å).[30] This noticeable error is typical for both the GGA and LDA functional. Obviously, we infer that, for the lattice constants a and c of $MgSiP_2$, the best agreement with experiment is

Table II. Calculated elastic constants (C_{ij}), bulk modulus (B), shear modulus (G), B/G ratio, and Poisson's ratio (υ)

Compound	Reference	C_{11}	C_{12}	C_{13}	C_{33}	C_{44}	C_{66}	B_V	B_R	B	G_V	G_R	G	B/G	υ
$MgSiP_2$	Present (LDA-CA)	132.482	60.994	71.0278	86.382	42.926	49.807	84.161	80.641	82.401	37.02	29.259	33.138	2.49	0.323
	Present (GGA-PW91)	118.102	51.560	60.93	81.179	39.882	47.296	73.803	71.892	72.847	35.01	29.222	32.116	2.27	0.308
	Present (GGA-PBE)	118.074	51.552	60.875	80.569	39.527	47.008	73.702	71.680	72.691	34.773	28.963	31.868	2.28	0.309
	Present (GGA-RPBE)	114.395	48.350	57.179	78.909	39.995	46.961	70.346	68.627	69.486	35.056	29.666	32.361	2.15	0.298
	Present (GGA-PBEsol)	123.375	55.211	65.706	77.756	35.698	45.799	77.528	73.682	75.605	32.631	25.540	29.085	2.60	0.330
	Present (GGA-AM05)	122.295	53.997	64.147	77.727	36.716	46.129	76.320	72.819	74.569	33.248	26.439	29.844	2.50	0.323
	Theory[12]	110.59	55.61	68.06	78.61	35.61	34.19								0.300
	Theory[20]	110.700	43.100	52.600	76.100	48.700	38.200			65.300			34.100	1.92	0.278
$MgSiAs_2$	Present (LDA-CA)	105.686	51.834	58.210	72.805	35.526	42.188	68.965	66.744	67.855	30.376	24.350	27.363	2.48	0.322
	Present (GGA-PW91)	93.506	42.241	48.559	68.180	32.926	37.980	59.324	58.293	58.808	28.489	24.450	26.469	2.22	0.304
	Present (GGA-PBE)	93.283	42.061	48.370	67.650	32.653	37.750	59.091	58.016	58.553	28.305	24.274	26.290	2.23	0.305
	Present (GGA-RPBE)	89.518	38.954	44.665	65.537	32.800	37.235	55.682	54.765	55.224	28.320	24.654	26.487	2.08	0.293
	Present (GGA-PBEsol)	99.153	46.151	53.626	67.495	30.442	37.799	63.623	61.648	62.635	27.230	22.320	24.775	2.53	0.325
	Present (GGA-AM05)	98.100	44.720	51.917	67.278	31.399	38.048	62.287	60.508	61.397	27.831	23.143	25.487	2.41	0.318
	Theory[20]	102.60	42.600	51.300	69.100	45.900	42.300			61.900			31.600	1.96	0.282
$MgSiSb_2$	Present (LDA-CA)	71.620	39.836	43.591	58.644	23.910	28.488	50.658	50.310	50.484	20.253	17.079	18.666	2.70	0.335
	Present (GGA-PW91)	65.900	33.610	36.000	53.605	23.843	26.157	44.069	43.721	43.895	20.089	17.827	18.958	2.32	0.311
	Present (GGA-PBE)	65.669	33.432	35.809	53.253	23.706	26.011	43.854	43.495	43.675	19.987	17.740	18.864	2.31	0.311
	Present (GGA-RPBE)	62.634	30.520	32.556	51.116	23.835	25.720	40.850	40.543	40.696	19.958	17.945	18.951	2.15	0.298
	Present (GGA-PBEsol)	69.839	37.338	40.179	54.416	22.464	25.875	47.720	47.084	47.402	19.254	16.712	17.983	2.64	0.332
	Present (GGA-AM05)	68.812	35.670	38.307	54.067	23.342	26.243	46.250	45.702	45.976	19.879	17.459	18.669	2.46	0.321
	Theory[20]	81.500	37.400	42.400	61.900	35.500	30.900			51.800			25.100	2.06	0.291

The subscripts "V" and "R" denote the Voigt and Reuss approximations for $MgSiX_2$ (X = P, As, Sb) for different exchange–correlation functionals. The elastic constants, bulk modulus (B), and shear modulus (G) are expressed in GPa, while the B/G ratio and Poisson's ratio (υ) are dimensionless.

obtained using the AM052 calculations.[6] It is also noticeable that the result for the lattice constant a is very similar for the AM05 and PBEsol functionals.[27] It should be stated here that both PBEsol and AM05 give reliable results for structural properties, as shown in Ref. 31. Unfortunately, no experimental data for the lattice constants or bulk modulus of $MgSiAs_2$ or $MgSiSb_2$ are available in literature to discuss which exchange–correlation functional gives better results. We noticed a small mismatch with respect to other computational studies.[11,18–20] From Table I, the order of the lattice constants from low to high is: LDA < AM05 ≤ PBEsol < PW91 < PBE < RPBE for $MgSiP_2$ and LDA < PBEsol < AM05 < PW91 < PBE < RPBE for $MgSiAs_2$ and $MgSiSb_2$. The obtained bulk modulus (Table I) predicts an order of RPBE < PBE < PW91 < AM05 < PBEsol < LDA for each compound. The calculated dB/dP is reasonable compared with other theoretical studies, with deviation nearly less than 10% compared with Ref. 11 and 9% compared with Ref. 9.

Mechanical Properties

The elastic constants of a material provide fundamental useful information about its mechanical properties. The results of our calculations were obtained using the "stress–strain method."[32,33] We predicted many useful mechanical properties, namely the bulk modulus B, shear modulus G, Poisson's ratio υ, and anisotropy factors, all derivable from the elastic constants. Details of the calculations and equations can be found elsewhere.[34–37] The results are summarized in Tables II and III together with other corresponding first-principles calculations. The positive values obtained for the six independent elastic constants indicate that all the title compounds are stable in this phase. As usual, the elastic constants obtained using the LDA are larger than those calculated using the GGA functionals. As can be seen from these tables, the values of the elastic constants increase in the following sequence: $C_{ij}(MgSiSb_2) < C_{ij}(MgSiAs_2) < C_{ij}(MgSiP_2)$. Similar studies to calculate the elastic properties were reported in Refs. 12 and 20. While the elastic constants calculated using the LDA have high error compared with Ref. 20, the results calculated using the GGA functionals, especially PBE and PW91, are consistent with Ref. 20. It is also found that the elastic constants lie in the order LDA > PBEsol > AM05 > PW91 > PBE > RPBE for each compound. It is important to note that all the investigated GGA functionals provide similar results to one another. In particular, the values of the elastic properties obtained using the PW91 and PBE functionals were highly similar; These values decrease with the size of the anion atom from P to Sb. It is noticed that C_{11} is larger than C_{33}, indicating that the c-axis is more compressible than the a-axis for each compound. Also, C_{44} is lower than C_{66}, indicating that shear along the (001) plane is easier than shear along the (100) plane.

The bulk modulus measures the resistance to volume change for constant shape.[38] For these compounds, the bulk modulus increases in the order: $B(MgSiSb_2) < B(MgSiAs_2) < B(MgSiP_2)$. We conclude that the bulk modulus calculated from the elastic constants within the Voigt–Reuss–Hill

Table III. Shear anisotropy factors A^a and A^c, percentage of elastic anisotropy for bulk modulus A_{comp} and shear modulus A_{shear} (%), and universal anisotropy index A^u of $MgSiX_2$ (X = P, As, Sb) calculated for several exchange–correlation functionals

Compound	Present	A^a	A^c	A_{comp}	A_{shear}	A^u
$MgSiP_2$	LDA-CA	2.24	1.39	2.14	11.71	1.37
	GGA-PW91	2.06	1.42	1.31	9.01	1.02
	GGA-PBE	2.06	1.41	1.39	9.12	1.03
	GGA-RPBE	2.03	1.42	1.24	8.33	0.93
	GGA-PBEsol	2.05	1.34	2.54	12.19	1.44
	GGA-AM05	2.05	1.35	2.35	11.41	1.34
	Theory[20]	2.39	1.13			
$MgSiAs_2$	LDA-CA	2.29	1.57	1.63	11.01	1.27
	GGA-PW91	2.04	1.48	0.88	7.63	0.84
	GGA-PBE	2.03	1.47	0.92	7.67	0.85
	GGA-RPBE	2.00	1.47	0.83	6.92	0.76
	GGA-PBEsol	2.05	1.43	1.58	9.91	1.13
	GGA-AM05	2.04	1.43	1.45	9.20	1.04
	Theory[20]	2.66	1.41			
$MgSiSb_2$	LDA-CA	2.22	1.79	0.34	8.50	0.94
	GGA-PW91	2.01	1.62	0.40	5.96	0.64
	GGA-PBE	2.00	1.61	0.41	5.96	0.64
	GGA-RPBE	1.96	1.57	0.38	5.31	0.57
	GGA-PBEsol	2.05	1.59	0.67	7.07	0.77
	GGA-AM05	2.02	1.58	0.59	6.48	0.70
	Theory[20]	2.42	1.40			

approximation[39–41] matches with that obtained from the total energy minimization calculation (Table I) for each compound. The order of the bulk modulus values calculated using the various functionals in the present work is consistent with that of the elastic constants. The shear modulus, a measurement of the resistance to shape change, is more pertinent to hardness,[38] and high shear modulus is mainly due to larger C_{44}. The mechanical properties of a material are usually classified into two main types, namely brittle and ductile, based on the B/G ratio.[42] If this ratio is smaller than 1.75, then the material is brittle, whereas a value of B/G higher than 1.75, as in these compounds, indicates a ductile material. From Table II, it is clear that the B/G ratio calculated for all the investigated compounds was larger than 1.75, therefore predicting ductile nature, for all the functionals. Moreover, the ductile nature of all the investigated compounds is confirmed by their positive Cauchy pressures ($C_{13} - C_{44} > 0$, $C_{12} - C_{66} > 0$).[43,44]

The Poisson's ratio (υ) provides more information about the characteristics of the bonding forces than any of the other elastic constants. The lower and upper limits of the Poisson's ratio υ are given as 0.25 and 0.50 for central forces in solids, respectively.[45] It should be noted that the obtained values of υ are about 0.298 to 0.335, suggesting that interatomic forces are central in these compounds. The brittle or ductile nature of a material can also be determined from the Poisson's ratio.[46] The values calculated for these compounds (Table II) are smaller than ~0.33, confirming their ductile nature.

One further point of interest is the shear anisotropy, an important property representing the degree of elastic anisotropy in a solid. Our calculated results are presented in Table III. For tetragonal structure, the shear anisotropy factors A^a in the {100} plane and A^c in the {001} plane are given by the following equations, respectively[20,45,47]:

$$A^a = \frac{4C_{44}}{(C_{11} + C_{33} - 2C_{13})}, \quad (1)$$

$$A^c = \frac{2C_{66}}{(C_{11} - 2C_{12})}. \quad (2)$$

The calculated anisotropy factor values in Table III indicate that these compounds have a certain anisotropy in both the {100} and {001} planes for this crystal structure. It is also revealed that the c-axis anisotropy factor is smaller than that for the a-axis.

We also calculated the percentage elastic anisotropy for the polycrystalline materials, defined as $A_{comp} = [(B_V - B_R)/(B_V + B_R)]$ and $A_{shear} = [(G_V - G_R)/(G_V + G_R)]$ for compressibility and shear, respectively.[37,47,48] In these equations, the subscripts "V" and "R" indicate the Voigt and Reuss approximations, respectively. The calculated results for A_{comp} (in %) and A_{shear} (in %) are presented in Table III. From these results, we conclude that these compounds exhibit large elastic anisotropy in shear but small elastic anisotropy in compressibility. The obtained values of A_{comp} and A_{shear} decrease as the X atom is changed from P to Sb. It may also be noted that the value of A_{comp} obtained for the compound $MgSiSb_2$ is about 0.34 to 0.67, indicating that the $MgSiSb_2$ compound is slightly isotropic in compressibility, as a value of 0% corresponds to elastic isotropy whereas a value of 100% identifies the largest elastic anisotropy.

Another important elastic anisotropy factor is the universal anisotropy index A^u,[49] calculated using the relation $A^u = [5(G_V/G_R) + (B_V/B_R)] - 6$. If A^u is equal to zero, elastic isotropy exists, while deviations of A^u from zero indicate elastic anisotropy. Our results for these compounds for all the investigated functionals suggest that they exhibit elastic anisotropy.

Thermophysical Properties

Adjustment of the thermal properties of a material can have a variety of benefits in applied science. Here, we discuss the thermophysical properties of all the considered compounds at high pressure/temperature calculated using the GGA-AM05 functional, which gave better results than the others for the lattice constants of the compound $MgSiP_2$. The calculations were performed using the quasiharmonic Debye model as implemented in the GIBBS code.[50] This approach allows one to discussion the pressure/temperature dependence of important thermal properties of the compounds. Detailed description of the theoretical background can be found in Refs. 51–53. The energy–volume data allow us to predict the thermal properties. Based on our estimated results, the dependence of the equation of state (EOS) data can provide reliable predictions to explain basic thermal quantities such as the normalized volume (V/V_0), bulk modulus (B), linear thermal expansion (α), Debye temperature (θ), and Grüneisen parameter (γ) in detail. Due to the lack of experimental data, our *ab initio* study will provide insightful information on the thermophysical properties of $MgSiX_2$ (X = P, As, Sb) at high pressure and temperature.

Throughout this section, we discuss the temperature and pressure dependence of the thermal properties of each compound in the temperature range from 0 K to 1000 K and for pressures up to 25 GPa. Even though all the computed results presented below seem to be identical, the obtained values present small discrepancies. The dependence of the normalized volume V/V_0 on temperature and pressure is shown in Fig. 2a–c. It should be noted that V/V_0 decreases with increasing pressure at constant temperature. It is also seen that V/V_0 tends to decrease with increasing temperature at constant pressure, albeit at a very moderate rate.

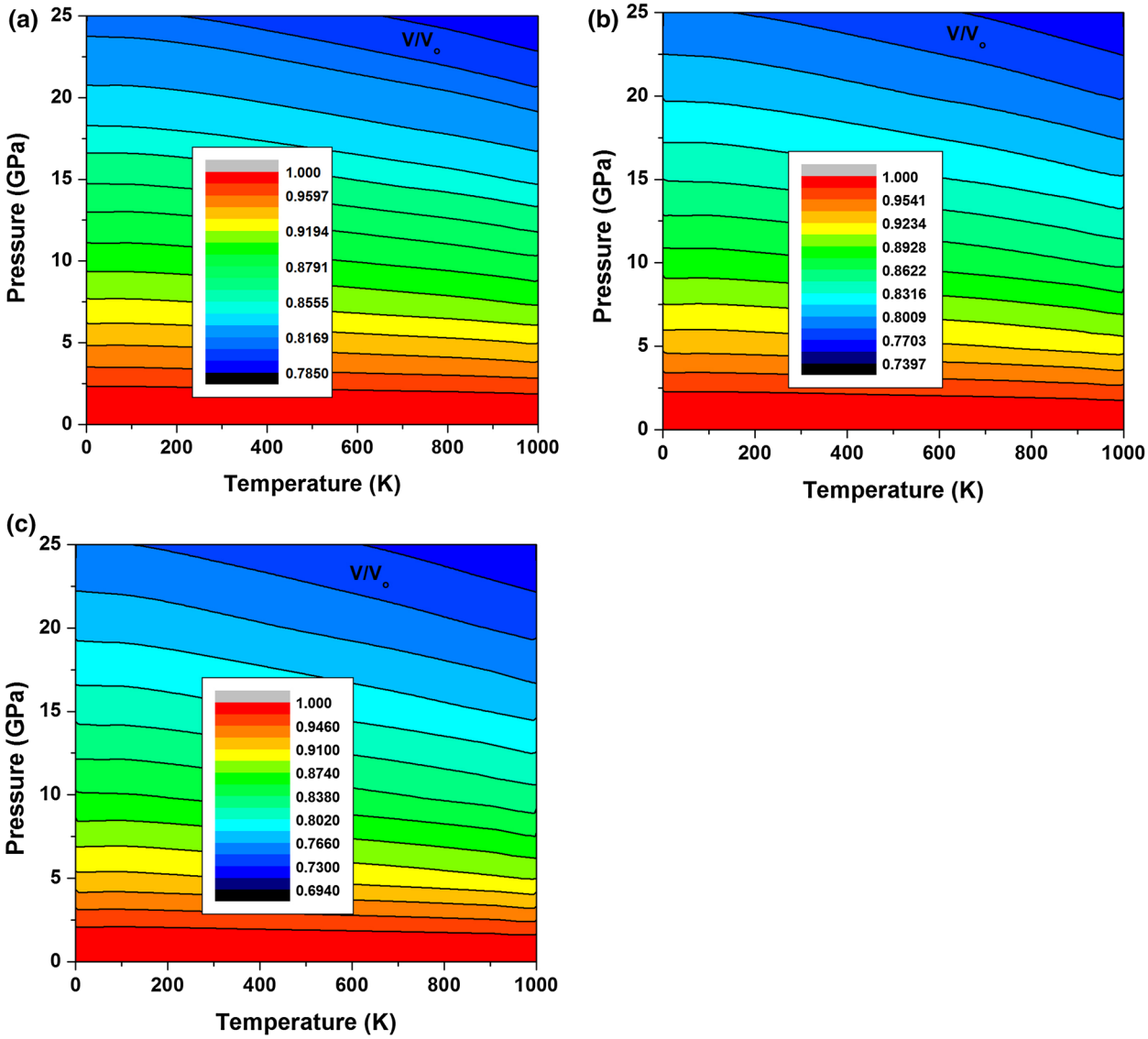

Fig. 2. Contours of normalized volume V/V_0 versus pressure (P in GPa) and temperature (T in K) calculated for (a) $MgSiP_2$, (b) $MgSiAs_2$, and (c) $MgSiSb_2$.

Figure 3a–c presents the calculated bulk modulus (B) as a function of temperature and pressure for each compound. It is noticeable that the calculated zero-pressure and zero-temperature value of B (76.57 GPa for MgSiP,[2,62] 49 GPa for $MgSiAs_2$, and 46.25 GPa for $MgSiSb_2$) is compatible with those obtained from both the Murnaghan equations (Table I) and the Voigt–Reuss–Hill approximation (Table II) using the AM05 functional. At temperature of 300 K and zero pressure, B is found to be 73.2 GPa, 58.8 GPa, and 42.95 GPa for $MgSiX_2$ with X = P, As, and Sb, respectively. $MgSiP_2$ has the highest B value among these compounds, while $MgSiSb_2$ has the lowest value over the whole temperature range. It is clearly seen that B increases with pressure at constant temperature, while B decreases with temperature at constant pressure. It is important to note that the effect of pressure on the bulk modulus is greater than that of temperature.

The thermal expansivity is a very important parameter for interpreting the thermodynamic and thermoelastic behavior of solids at high temperature. The dependence of the thermal expansion coefficient (α) on temperature and pressure is depicted in Fig. 4a–c. From Fig. 4, we find $\alpha^{MgSiP_2} < \alpha^{MgSiAs_2} < \alpha^{MgSiSb_2}$ at all pressures. It is concluded that α decreases with increasing pressure at constant temperature. Furthermore, the effect of pressure on α is slight below 100 K, although the effect of pressure is enhanced with increasing pressure. At constant pressure, α increases with increasing temperature. It can be seen that α increases quickly below temperature of 300 K at zero pressure. After a sharp increase, α becomes nearly insensitive to temperature, and the

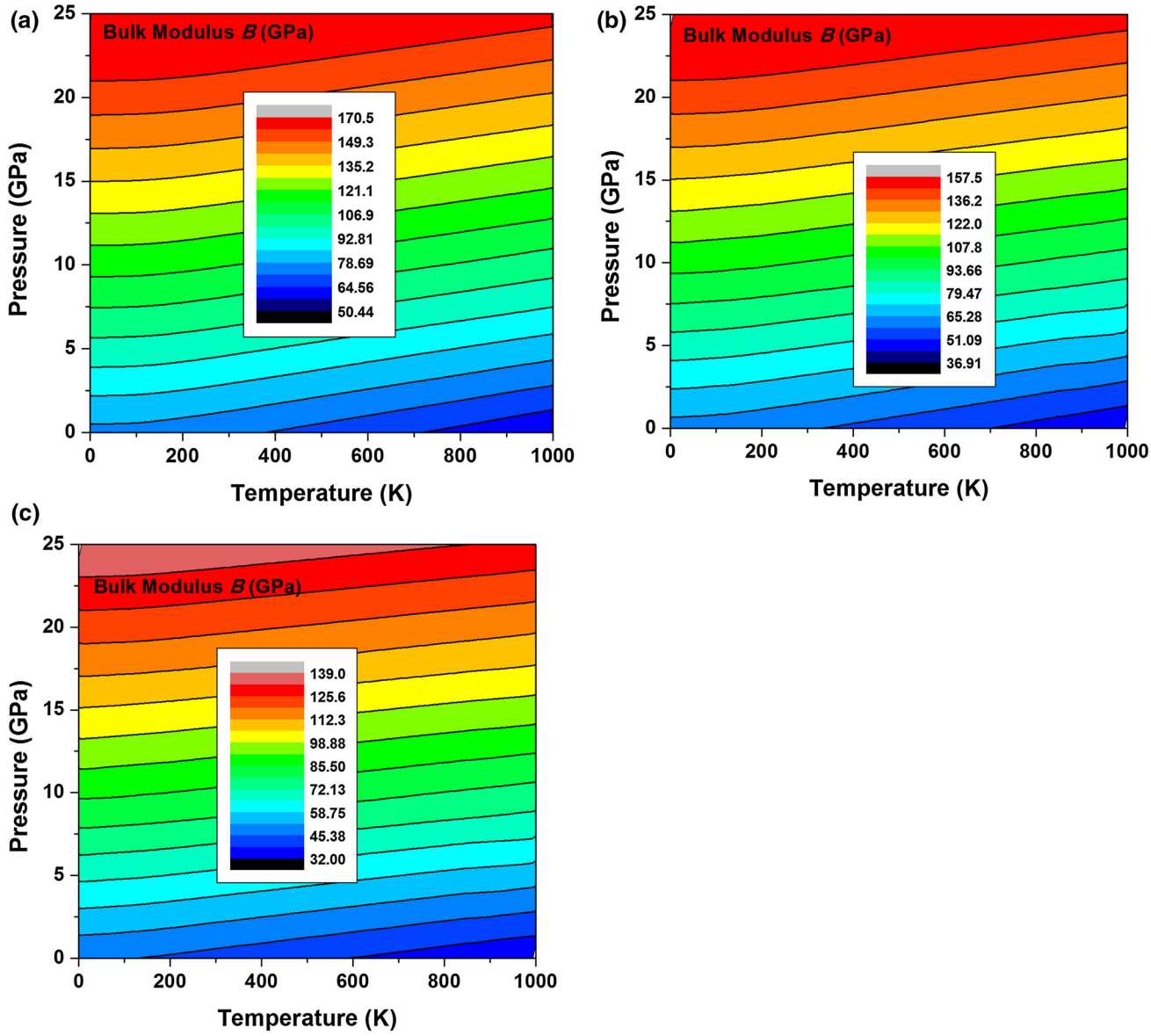

Fig. 3. Contours of bulk modulus (B in GPa) versus temperature (T in K) and pressure (P in GPa) calculated for (a) $MgSiP_2$, (b) $MgSiAs_2$, and (c) $MgSiSb_2$.

increasing trend becomes moderate at higher temperatures.[54]

The variation of the heat capacity at constant volume (C_V) with temperature and pressure is plotted in Figs. 5a–c and 6a–c for these compounds. From Figs. 5 and 6, while at lower temperatures/pressures ($\sim T < 300$ K) C_V is strongly dependent on both pressure and temperature, at higher temperatures/pressures C_V reaches the classical Dulong–Petit limit, a generally known tendency. C_V increases from P to As to Sb (163.04 J mol^{-1} K^{-1}, 180.36 J mol^{-1} K^{-1}, and 188.96 J mol^{-1} K^{-1}, respectively) at 300 K and zero pressure. We also observe that temperature has a strong influence on C_V, being the most noticeable point for these graphs.

The Debye temperature (θ), another thermal property important for material design, is reported in Fig. 7a–c. The calculated values of θ are 616.4 K, 431.3 K, and 315.1 K at 300 K for $MgSiP_2$, $MgSiAs_2$, and $MgSiSb_2$, respectively. On changing the anion atom X from P to Sb, the value of θ decreases. Moreover, it is seen that the increase of θ with applied pressure at constant temperature is almost linear. Another important point regarding the Debye temperature is that it decreases with increasing temperature at constant pressure, in agreement with the bulk modulus graphs.

Finally, the effect of temperature/pressure on the Grüneisen parameter (γ) is illustrated in Fig. 8a–c. The Grüneisen parameter defines the effect of a change of volume on the dynamics of the crystal

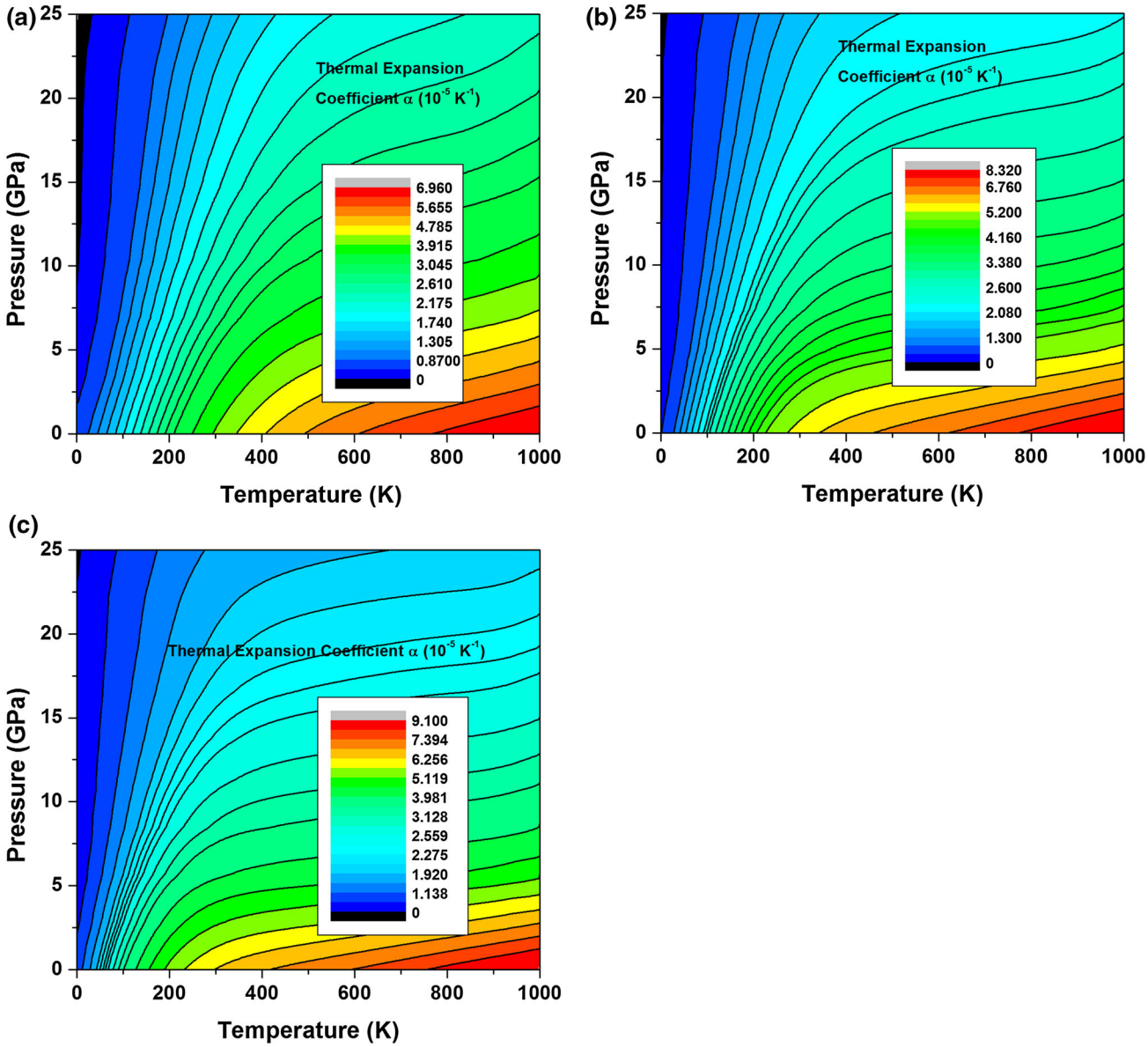

Fig. 4. Contours of linear thermal expansion coefficient (α in 10^{-5} K^{-1}) versus temperature (T in K) and pressure (P in GPa) calculated for (a) $MgSiP_2$, (b) $MgSiAs_2$, and (c) $MgSiSb_2$.

lattice. The Grüneisen parameter at 300 K and 0 GPa was calculated as 2.04, 2.09, and 2.14 for $MgSiP_2$, $MgSiAs_2$, and $MgSiSb_2$, respectively. We observed that the value of γ remains constant at low temperatures, but at higher temperatures it increases almost linearly with temperature for these compounds. It should be noted that γ decreases with increasing pressure at constant temperature.

Electronic Properties

The electronic band structure calculated along several high-symmetry directions in the first Brillouin zone and the related partial density of states (PDOS) for the $MgSiX_2$ compounds with X = P, As, and Sb are presented for the body-centered tetragonal structure in Fig. 9a, b, and c, respectively. As seen in Fig. 9a–c, as the conduction-band minimum and valence-band maximum are located at the Γ point, all three compounds are direct-bandgap semiconductors. This implies that they may be candidates for use in photonic device applications instead of III–V compounds. The values of the bandgap (E_g) of the considered chalcopyrites are collected in Table IV. Clearly, these values calculated using the LDA and GGA functionals are lower than experimental values, with the best overall description being provided by the GGA-RPBE method for the $MgSiP_2$ and $MgSiAs_2$ compounds and GGA-AM05 for $MgSiSb_2$. This deficiency is generally expected when applying pure DFT.

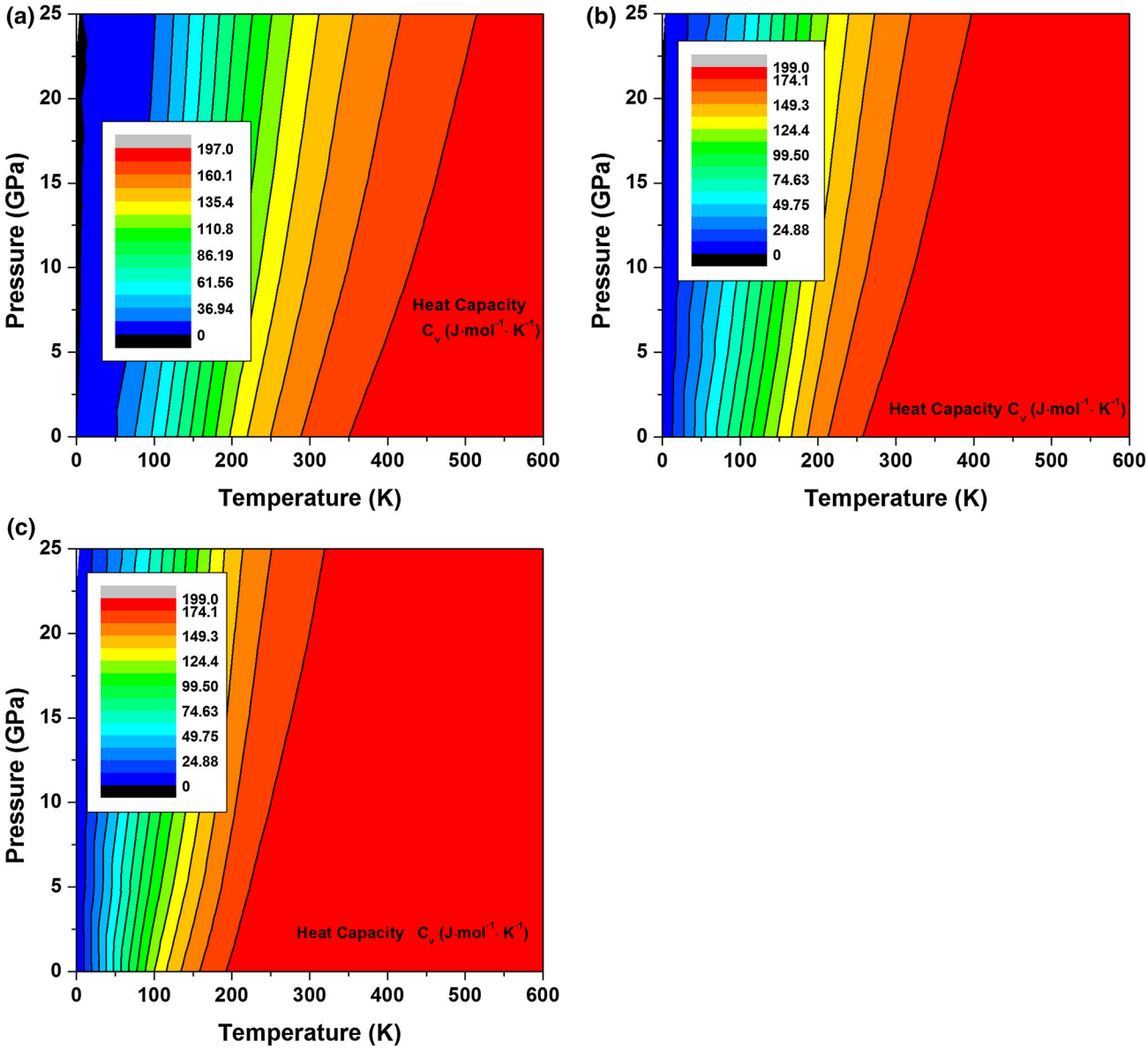

Fig. 5. Contours of heat capacity (C_V in J mol^{-1} K^{-1}) versus temperature (T in K) and pressure (P in GPa) calculated for (a) $MgSiP_2$, (b) $MgSiAs_2$, and (c) $MgSiSb_2$.

Shaposhnikov et al.[18] used the modified Becke–Johnson (mBJ) potential and GW approximation to obtain accurate results for the electronic band structure and optical properties of these compounds. It seems that the mBJ method is successful in overcoming this problem. Moreover, similar investigations on first-principles study of some materials are reported in Refs. 11 and 19. The choice of several exchange–correlation potentials in the projector augmented-wave (PAW) formalism also seems to influence the E_g results, but all the exchange–correlation functionals considered herein are inadequate for accurate prediction of E_g. We decided to use the GGA-RPBE functional for $MgSiP_2$ and $MgSiAs_2$ and the GGA-AM05 functional for $MgSiSb_2$ hereinafter for the electronic and optical properties.

As shown in Fig. 9a–c (right side), whereas the occupied part of the valence band can be subdivided into three regions, the conduction band has one part. The first and lowest-lying states between about −12.5 eV and −9 eV mainly originate from anion (P, As, Sb) s-states with a minor contribution from a mixture of Si s- and p-states, whereas the higher energy range between about −7.5 eV and −5 eV is mainly due to Si and anion atom (P, As, Sb) s- and p-states. The PDOS in the region from −4.5 eV to 0 eV is mainly constructed from anion atom (P, As, Sb) p-states with Si p-states. The conduction band is formed by Si and anion atom (P, As, Sb) s- and p-states.

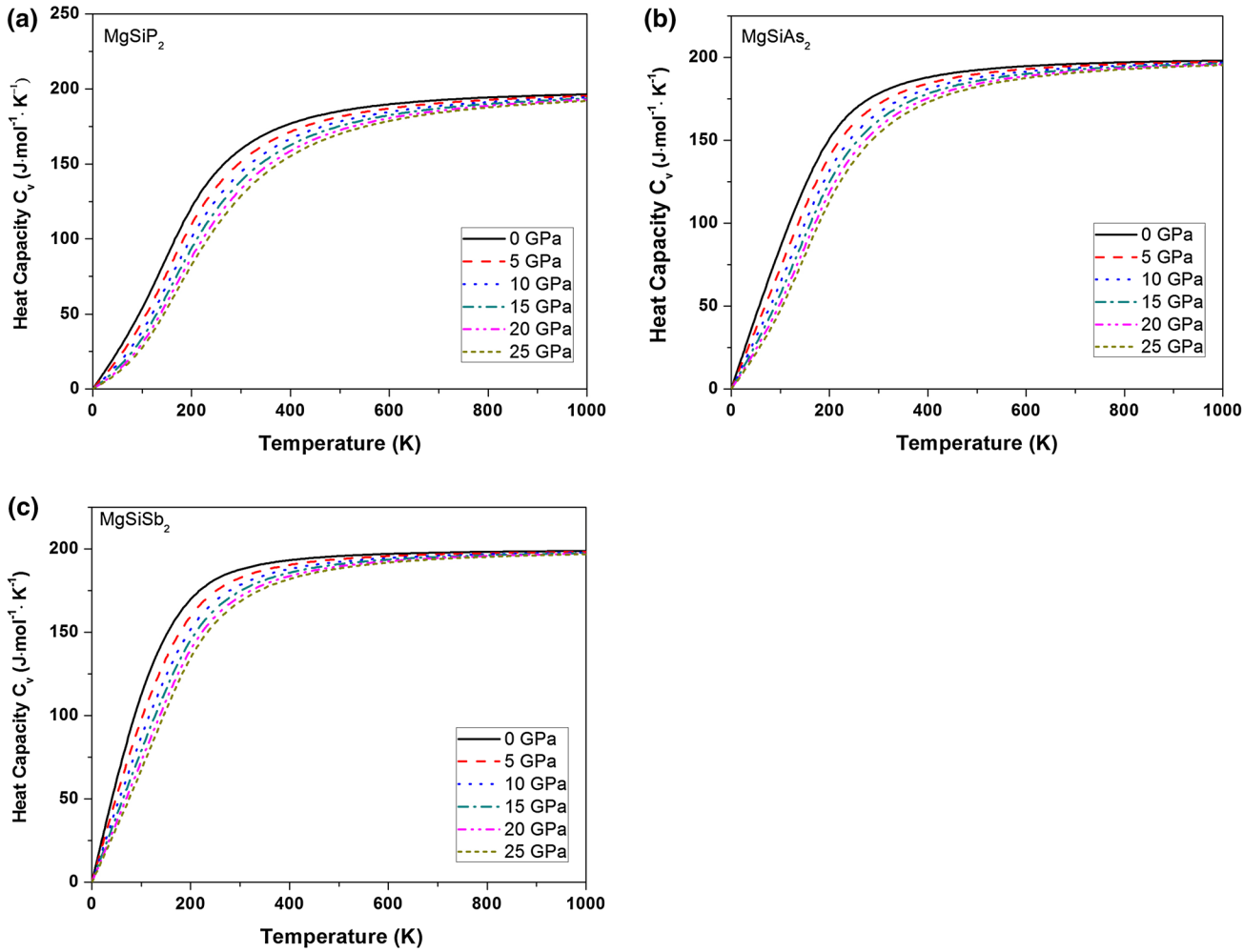

Fig. 6. Heat capacity at constant volume calculated as a function of temperature (T in K) at various pressures (P in GPa) for (a) $MgSiP_2$, (b) $MgSiAs_2$, and (c) $MgSiSb_2$.

To obtain detailed understanding of the interaction among the different atomic orbitals, we present contour plots of the charge density in the (100) plane of $MgSiX_2$ (X = P, As, Sb) in Fig. 10. The overall charge density contour profiles are quite similar for all the compounds, with small differences in the details, and these results are compatible with earlier studies.[4,6,19] It can be concluded that charge is shared between Si and anion (X = P, As, Sb) atoms, indicating the covalent nature of the Si–X bond. Furthermore, the spherical charge distribution indicates that the bonding interaction between Mg and X (X = P, As, Sb) has ionic character. Thus, the bonding nature for all three compounds can be characterized as mixed ionic–covalent. It can also be seen that our charge density maps are compatible with the PDOS analysis.

Optical Properties

We start the discussion of the optical properties of these compounds by deriving the complex dielectric function $\varepsilon(\omega) = \varepsilon_1(\omega) + i\varepsilon_2(\omega)$. The imaginary part of the dielectric function $\varepsilon_2(\omega)$ represents the optical absorption by the crystal, which can be calculated from the momentum matrix elements between occupied and unoccupied states as follows:

$$\varepsilon_2(\omega) = \frac{Ve^2}{2\pi\hbar m^2\omega^2}\int \mathrm{d}^3k \sum_{n,n'} \left|\left\langle kn|p|kn'\right\rangle^2\right| f(kn)(1-f(kn'))\delta(E_{kn}-E_{kn'}-\hbar\omega), \quad (3)$$

where e is the electronic charge, V is the unit cell volume, p is the momentum operator, $|kn\rangle$ is a crystal wavefunction, $f(kn)$ is the Fermi distribution function, and $\hbar\omega$ is the energy of the incident photon. The real part $\varepsilon_1(\omega)$ can be evaluated from the Kramers–Kronig relationship as

$$\varepsilon_1(\omega) = 1 + \frac{2}{\pi}M\int_0^\infty \frac{\varepsilon_2(\omega')\omega'}{\omega'^2-\omega^2}\mathrm{d}\omega, \quad (4)$$

where M is the principal value of the integral.[58–62] The optical constants calculated using the different exchange–correlation functionals are presented in

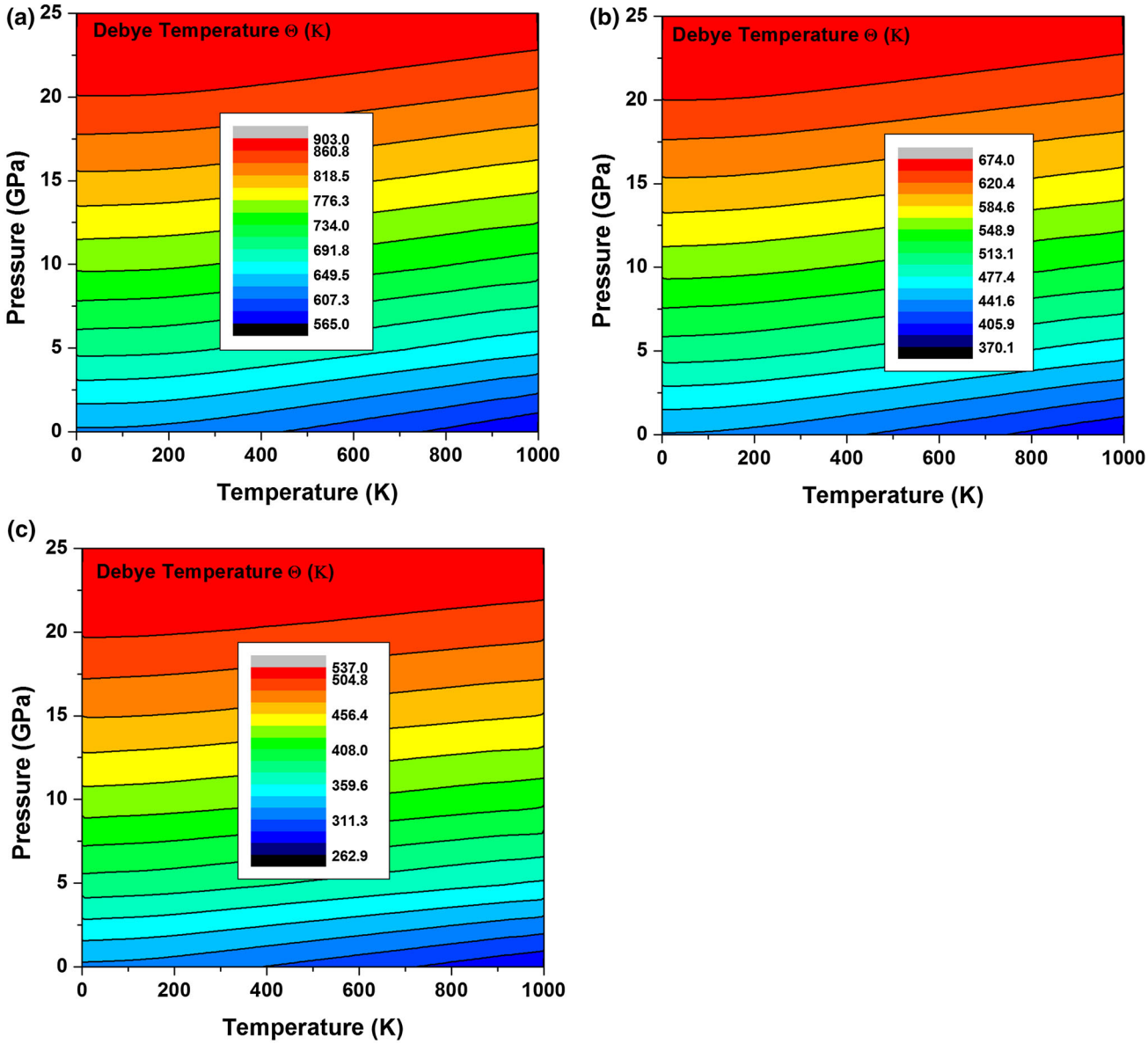

Fig. 7. Contours of Debye temperature (θ in K) versus temperature (T in K) and pressure (P in GPa) calculated for (a) $MgSiP_2$, (b) $MgSiAs_2$, and (c) $MgSiSb_2$.

Table V together with results from other available theoretical studies. We can say that the use of the different exchange–correlation functionals did not affect the results substantially (Table V).

The calculated real $\varepsilon_1(\omega)$ and imaginary $\varepsilon_2(\omega)$ parts of the dielectric function $\varepsilon(\omega)$ as a function of photon energy are illustrated in Fig. 11a and b from 0.0 eV to 15 eV. Since the $MgSiX_2$ (X = P, As, Sb) compounds are body-centered tetragonal, they are characterized by two principal tensor components, perpendicular and parallel to the c-axis of the dielectric tensor. As shown in Fig. 11, there is considerable anisotropy between the perpendicular and parallel dielectric tensors. It is clearly seen that, as one changes from P $\rightarrow$ As $\rightarrow$ Sb, the peaks in $\varepsilon_1(\omega)$ shift to the low energy region and the static real dielectric function increases for each functional. For energies larger than about 5.1 eV, 4.7 eV, and 3.8 eV, the real part becomes negative for $MgSiP_2$, $MgSiAs_2$, and $MgSiSb_2$, indicating that these compounds exhibit metallic nature, because incident electromagnetic waves are totally

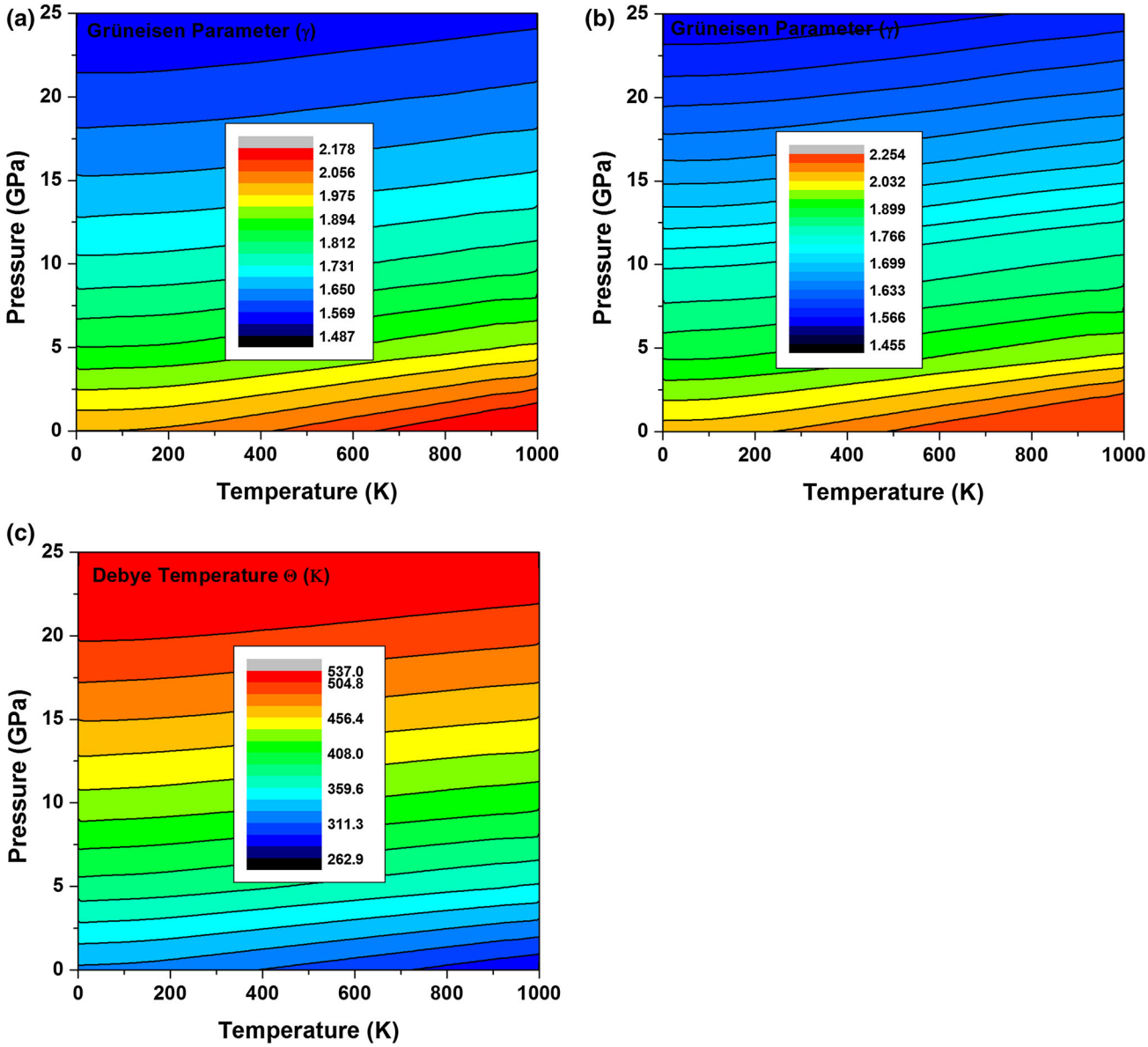

Fig. 8. Contours of Grüneisen parameter (γ) versus temperature (T in K) and pressure (P in GPa) calculated for (a) $MgSiP_2$, (b) $MgSiAs_2$, and (c) $MgSiSb_2$.

reflected by the medium in these energy regions.[58,62]

As can be seen from Fig. 11b, the dominant peak of the imaginary part of the dielectric function $\varepsilon_2\perp(\omega)$ is located at 4.41 eV, 4.21 eV, and 3.57 eV for $MgSiP_2$, $MgSiAs_2$, and $MgSiSb_2$, respectively. $\varepsilon_{2//}(\omega)$ also shows peaks, at 4.313 eV, 3.59 eV, and 3.0 eV for $MgSiP_2$, $MgSiAs_2$, and $MgSiSb_2$, respectively, which are related to interband transitions between valence and conduction band. This figure clearly indicates that the maximum peak for these compounds shifts to lower energy as the value of E_g decreases from $MgSiP_2 \rightarrow MgSiAs_2 \rightarrow MgSiSb_2$. However, no experimental studies on the optical properties of these compounds exist.

The values obtained for the complex dielectric function enable us to predict the refractive index $n(\omega)$, extinction coefficient $k(\omega)$, reflectivity $R(\omega)$, and energy loss function $L(\omega)$ with the aid of the Kramers–Kronig relations,[61–63] as given by the following expressions:

$$R(\omega) = \left(\frac{(n(\omega)-1)^2 + k(\omega)^2}{(n(\omega)+1)^2 + k(\omega)^2}\right), \quad (5)$$

$$n(\omega) = \left(\frac{\sqrt{\varepsilon_1^2(\omega) + \varepsilon_2^2(\omega)} + \varepsilon_1(\omega)}{2}\right)^{1/2}, \quad (6)$$

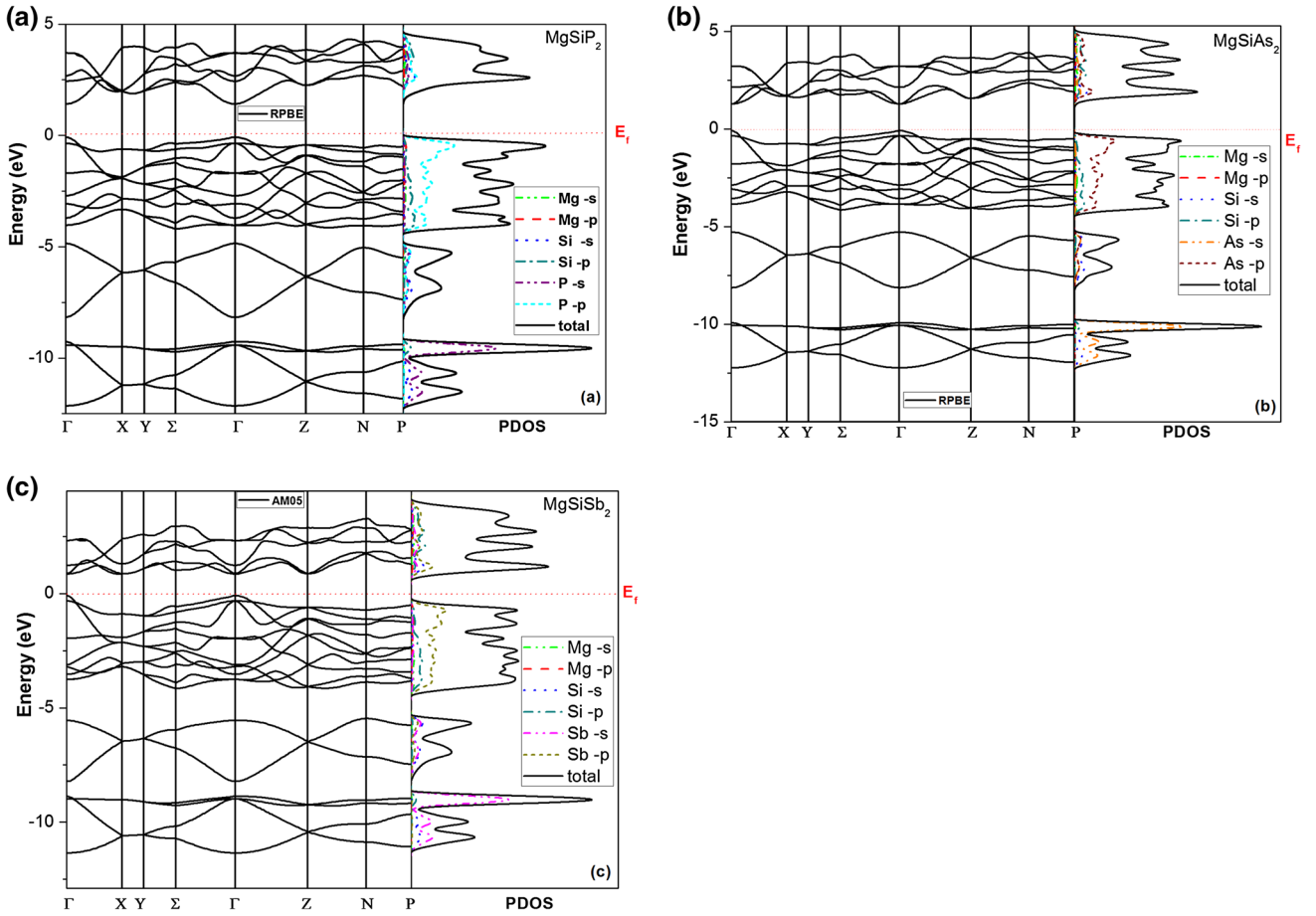

Fig. 9. Electronic band structure with partial and total density of states for (a) $MgSiP_2$ (RPBE), (b) $MgSiAs_2$ (RPBE), and (c) $MgSiSb_2$ (AM05).

Table IV. Bandgap energy (E_g, eV) of $MgSiX_2$ (X = P, As, Sb) compounds as calculated using various exchange–correlation functionals

	E_g (eV)							
		GGA						
Compound	**LDA**	**PW91**	**AM05**	**PBE**	**RPBE**	**PBEsol**	**Exp.**	**Other**
$MgSiP_2$	1.076	1.356	1.2	1.347	1.491	1.113	2.3[55] 3.50[16]	1.37[GGA18] 2.08[mBJ18] 1.83_0^{GW}[18] 1.15[15]
$MgSiAs_2$	1.000	1.238	1.119	1.231	1.373	1.027	2.67[16]	1.26[GGA18] 1.95[mBJ18] 1.40_0^{GW}[18] 2.00[5] 2.08[56]
$MgSiSb_2$	0.823	0.819	0.933	0.811	0.755	0.826	1.086[16]	1.22[15] 1.40[5] 1.39[56]

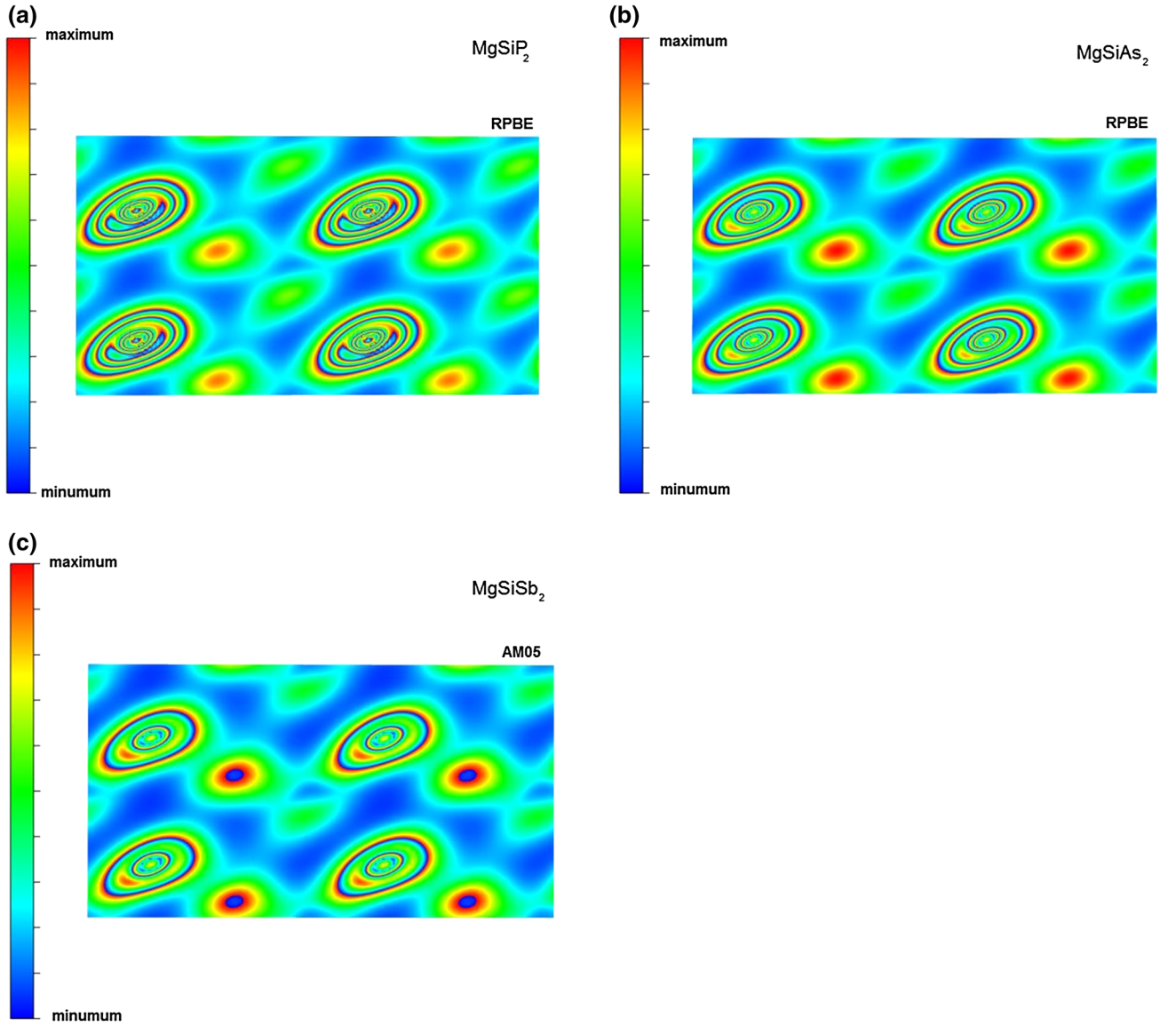

Fig. 10. Charge density in (100) plane for (a) $MgSiP_2$ (RPBE), (b) $MgSiAs_2$ (RPBE), and (c) $MgSiSb_2$ (AM05), drawn with VESTA package.[57]

$$k(\omega) = \left(\frac{\sqrt{\varepsilon_1^2(\omega) + \varepsilon_2^2(\omega)} - \varepsilon_1(\omega)}{2} \right)^{1/2}, \quad (7)$$

$$L(\omega) = \left(\frac{\varepsilon_2(\omega)}{\varepsilon_1^2(\omega) + \varepsilon_2^2(\omega)} \right). \quad (8)$$

The computed results for the title compounds are shown in Fig. 12a–d. The calculated refractive index is shown in Fig. 12a for all three compounds. The difference between the perpendicular and parallel refractive index clearly demonstrates optical anisotropy. The main peak value of the refractive index is found to be 4.5 at 2.97 eV for $MgSiP_2$, 4.35 at 2.34 eV for $MgSiAs_2$, and 4.9 at 1.5 eV for $MgSiSb_2$. As shown in Fig. 12b, the calculated maximum peak values of $k\perp(\omega)$ and $k_{//}(\omega)$ are located at 5.36 eV and 4.36 eV, 4.84 eV and 3.9 eV, and 3.2 eV and 3.1 eV for $MgSiP_2$, $MgSiAs_2$, and $MgSiSb_2$, respectively. The reflectivity spectra are plotted in Fig. 12c. Notice that both the static refractive index and static reflectivity increase as one changes the anion atom from P to Sb. It is found that the reflectivity of these compounds is high in

Table V. Calculated static real part of dielectric function [$\varepsilon_1\perp(0)$, $\varepsilon_{1//}(0)$], static refractive index [$n\perp(0)$, $n_{//}(0)$], static reflectivity [$R\perp(0)$, $R_{//}(0)$], static birefringence [$\Delta n(0)$], and plasmon frequency (ω_p in eV)

Compound	Reference	$\varepsilon_1\perp(0)$	$\varepsilon_{1//}(0)$	$n\perp(0)$	$n_{//}(0)$	$\Delta n(0)$	$R\perp(0)$	$R_{//}(0)$	ω_p
$MgSiP_2$	LDA-CA	11.363	11.442	3.371	3.383	0.012	0.294	0.296	18.65
	GGA-PW91	10.852	11.006	3.294	3.317	0.023	0.285	0.288	18.20
	GGA-PBE	10.902	11.041	3.302	3.323	0.021	0.286	0.289	18.67
	GGA-RPBE	10.566	10.745	3.250	3.278	0.03	0.280	0.284	18.14
	GGA-PBEsol	11.379	11.432	3.373	3.381	0.008	0.294	0.295	18.89
	GGA-AM05	11.157	11.232	3.340	3.351	0.01	0.291	0.292	18.67
	Theory[19]			2.826	2.952	0.126	0.228	0.244	
$MgSiAs_2$	LDA-CA	11.463	11.658	3.386	3.414	0.029	0.296	0.299	16.89
	GGA-PW91	11.346	11.668	3.368	3.416	0.047	0.294	0.299	17.04
	GGA-PBE	11.377	11.692	3.373	3.419	0.046	0.295	0.300	17.04
	GGA-RPBE	11.090	11.450	3.330	3.384	0.054	0.289	0.296	16.86
	GGA-PBEsol	11.609	11.802	3.407	3.435	0.028	0.298	0.301	17.15
	GGA-AM05	11.350	11.565	3.369	3.400	0.032	0.294	0.298	17.15
$MgSiSb_2$	LDA-CA	14.815	15.447	3.849	3.930	0.081	0.345	0.353	15.55
	GGA-PW91	14.574	15.624	3.817	3.907	0.089	0.342	0.351	15.35
	GGA-PBE	14.312	14.715	3.783	3.836	0.053	0.339	0.344	15.40
	GGA-RPBE	14.295	15.092	3.781	3.885	0.1	0.338	0.349	15.18
	GGA-PBEsol	14.772	15.230	3.843	3.903	0.06	0.345	0.351	15.57
	GA-AM05	14.315	14.745	3.784	3.840	0.06	0.339	0.344	15.55

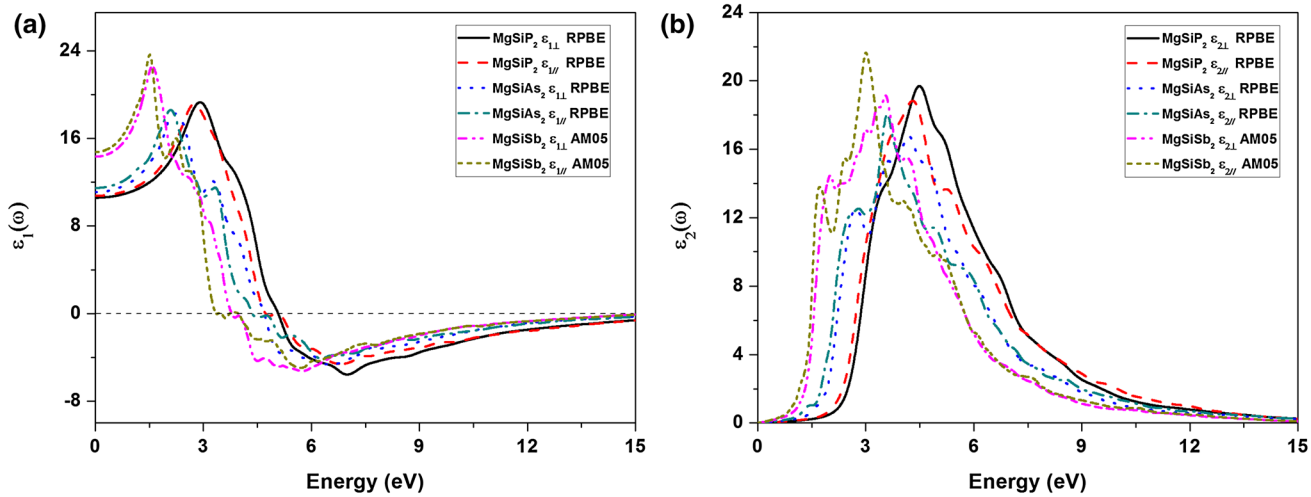

Fig. 11. Computed (a) real $\varepsilon_1(\omega)$ and (b) imaginary $\varepsilon_2(\omega)$ part of the dielectric function as a function of photon energy.

the ultraviolet–visible region up to nearly 16 eV (reaching their maximum at 14.5 eV to 16 eV), suggesting that these compounds may be promising candidates for use in optical devices such as ultraviolet radiation shields.

One further point of interest is the energy loss function, which is an important factor describing the energy loss of a fast electron traversing a material, shown in Fig. 12d for these compounds. The maximum peaks in the energy loss function

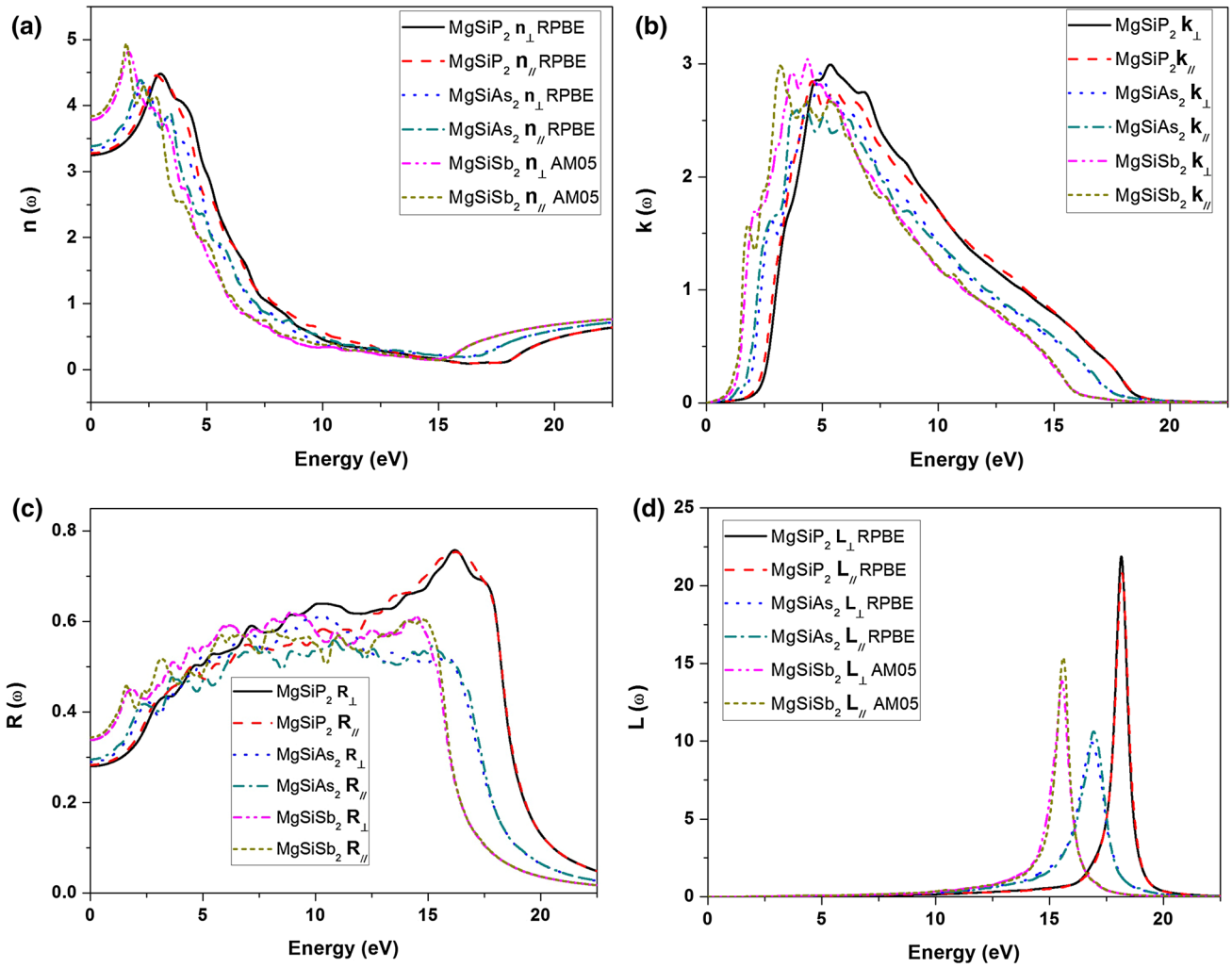

Fig. 12. Computed (a) refractive index $n(\omega)$, (b) extinction coefficient $k(\omega)$, (c) reflectivity $R(\omega)$, and (d) electron energy loss spectrum $L(\omega)$ as a function of photon energy.

give the plasmon frequency. The results indicate that the plasma frequency of $MgSiP_2$ is higher than for $MgSiAs_2$ or $MgSiSb_2$.

CONCLUSIONS

Ab initio density functional theory calculations were performed to obtain the general features of $MgSiX_2$ (X = P, As, Sb) compounds, revealing the effects of the six different exchange–correlation functionals applied. Unfortunately, none of the functionals could simultaneously estimate the electronic bandgap value well. We conclude that these compounds are direct-bandgap semiconductors, exhibiting ductile elastic nature and anisotropic behavior of both elastic and optical properties. The obtained elastic constant values are quite typical according to available literature. Changing the anion atom strongly affects all the properties for these compounds. Generally, we suggest that these compounds are quite favorable for use in thermophysical and nonlinear optical applications.

REFERENCES

1. J.L. Shay and J.H. Wernick, *Ternary Chalcopyrite Semiconductors: Growth, Electronic Properties, and Applications* (Oxford: Pergamon, 1975), pp. 1–254.
2. S.R. Römer, P. Kroll, and W. Schnick, *J. Phys. Condens. Matter* 21, 275407 (2009).
3. J.E. Jaffe and A. Zunger, *Phys. Rev. B* 27, 5176 (1983).
4. J.L. Martins and A. Zunger, *Phys. Rev. B* 32, 2689 (1985).
5. J.E. Jaffe and A. Zunger, *Phys. Rev. B* 29, 1882 (1984).
6. J.E. Jaffe and A. Zunger, *Phys. Rev. B* 30, 741 (1984).
7. S.Y. Sarkisov and S. Picozzi, *J. Phys. Condens. Matter* 19, 016210 (2007).
8. P. Zapol, R. Pandey, M. Seel, J.M. Recio, and M.C. Ohmer, *J. Phys. Condens. Matter* 11, 4517 (1999).
9. A.G. Petukhov, W.R.L. Lambrecht, and B. Segall, *Phys. Rev. B* 49, 4549–4558 (1994).
10. V. Kumar, S.K. Tripathy, V. Jha, and B.P. Singh, *Phys. Lett. A* 378, 519 (2014).
11. T. Ouahrani, *Eur. Phys. J. B* 86, 369 (2013).
12. T. Ouahrani, Y.Ö. Çiftci, and M. Mebrouki, *J. Alloys Compd.* 610, 372 (2014).
13. S.J. Park, Y. Cho, S.H. Moon, J.E. Kim, D.-K. Lee, J. Gwak, J. Kim, D.-K. Kim, and B.K. Min, *J. Phys. D Appl. Phys.* 47, 135105 (2014).

14. V.L. Shaposhnikov, A.V. Krivosheeva, F.A. D'Avitaya, J.-L. Lazzari, and V.E. Borisenko, *Phys. Stat. Sol. (b)* 245, 142 (2008).
15. F. Chiker, Z. Kebbab, R. Miloua, and N. Benramdane, *Solid State Commun.* 151, 1568 (2011).
16. C. Suh and K. Rajan, *Appl. Surf. Sci.* 223, 148 (2004).
17. S.C. Erwin and I. Žutić, *Nat. Mater.* 3, 410 (2004).
18. V.L. Shaposhnikov, A.V. Krivosheeva, V.E. Borisenko, J.-L. Lazzari, and F.A. d'Avitaya, *Phys. Rev. B* 85, 205201 (2012).
19. S. Ullah, G. Murtaza, R. Khenata, and A.H. Reshak, *Mater. Sci. Semicond. Process.* 26, 79 (2014).
20. L. Shi, J. Hu, Y. Qin, Y. Duan, L. Wu, X. Yang, and G. Tang, *J. Alloys Compd.* 611, 210 (2014).
21. M.V. Schilfgaarde, N. Newman, T.J. Peshek, T.J. Coutts, and T.A. Gessert, in *Photovoltaic Specialists Conference (PVSC), 34th IEEE* (2009), pp. 001297.
22. D.M. Ceperley and B.J. Alder, *Phys. Rev. Lett.* 45, 566 (1980).
23. J.P. Perdew and Y. Wang, *Phys. Rev. B* 45, 13244 (1992).
24. J.P. Perdew, K. Burke, and M. Ernzerhof, *Phys. Rev. Lett.* 77, 3865 (1996).
25. B. Hammer, L.B. Hansen, and J.K. Norskøv, *Phys. Rev. B* 59, 7413 (1999).
26. R. Armiento and A.E. Mattsson, *Phys. Rev. B* 72, 085108 (2005).
27. J.P. Perdew, A. Ruzsinszky, G.I. Csonka, O.A. Vydrov, G.E. Scuseria, L.A. Constantin, X. Zhou, and K. Burke, *Phys. Rev. Lett.* 100, 136406 (2008).
28. G. Kresse and D. Joubert, *Phys. Rev. B* 59, 1758 (1999).
29. G. Kresse and J. Hafner, *Phys. Rev. B* 47, 558 (1993).
30. A.A. Vaipolin, *Fiz. Tverd. Tela* 15, 1430 (1973). [*Sov. Phys. Solid State* 15, 965 (1973)].
31. M. Rasander and M.A. Moram, *J. Chem. Phys.* 143, 144104 (2015).
32. Y.L. Page and P. Saxe, *Phys. Rev. B* 65, 104104 (2002).
33. M.J. Mehl, J.E. Osburn, D.A. Papaconstantopoulos, and B.M. Klein, *Phys. Rev. B Condens. Matter* 41, 10311 (1990).
34. Z. Yang, X. Wang, L. Liu, S. Yang, and X. Su, *Solid State Sci.* 13, 1604 (2011).
35. S. Sharma, A.S. Verma, and V.K. Jindal, *Mater. Res. Bull.* 53, 218 (2014).
36. Z.-J. Wu, E.J. Zhao, H.P. Xiang, X.F. Hao, X.J. Liu, and J. Meng, *Phys. Rev. B* 76, 054115 (2007).
37. V.V. Bannikov, I.R. Shein, and A.L. Ivanovskii, *J. Alloys Compd.* 533, 71 (2012).
38. J.B. Levine, S.H. Tolbert, and R.B. Kaner, *Adv. Funct. Mater.* 19, 3519 (2009).
39. W. Voigt, *Lehrbuch der Kristallphysik,* 2nd ed. (Leipzig and Berlin: B.G. Teubner, 1910) [reprinted in 1928].
40. A. Reuss and Z. Angew, *Math. Mech.* 9, 49 (1929).
41. R. Hill, *Proc. R. Soc. Lond. Ser. A* 65, 349 (1952).
42. S.F. Pugh, *Philos. Mag.* 45, 823 (1954).
43. D.G. Pettifor, *Mater. Sci. Technol.* 8, 345 (1992).
44. I. Papadimitriou, C. Utton, A. Scott, and P. Tsakiropoulos, *Metall. Mater. Trans. A* 46, 566 (2015).
45. H. Fu, D. Li, F. Peng, T. Gao, and X. Cheng, *J. Alloys Compd.* 473, 255 (2009).
46. I. N. Frantsevich, F. F. Voronov, S. A. Bokuta, in *Elastic Constants and Elastic Moduli of Metals and Insulators Handbook,* ed. by I.N. Frantsevich (Naukova Dumka, Kiev, 1983), pp. 60–180.
47. P. Ravindran, L. Fast, P.A. Korzhavyi, and B. Johansson, *J. Appl. Phys.* 84, 4891 (1998).
48. D.H. Chung and W.R. Buessem, *Anisotropy in Single Crystal Refractory Compound,* vol 2, ed. by F.W. Vahldiek and S.A. Mersol (New York: Plenum, 1968), p. 217.
49. S.I. Ranganathan and M. Ostoja-Starzewski, *Phys. Rev. Lett.* 101, 055504 (2008).
50. M.A. Blanco, E. Francisco, and V. Luana, *Comput. Phys. Commun.* 158, 57 (2004).
51. E. Francisco, M.A. Blanco, and G. Sanjurjo, *Phys. Rev. B* 63, 094107 (2001).
52. S. Sharma, A.S. Verma, R. Bhandari, and V.K. Jindal, *Comput. Mater. Sci.* 26, 108 (2014).
53. B. Ai, X. Luo, J. Yu, W. Miao, and P. Hub, *Comput. Mater. Sci.* 82, 37 (2014).
54. X. Zha, S. Li, R. Zhang, and Z. Lin, *Commun. Comput. Phys.* 16, 201 (2014).
55. C.H.L. Goodman, *Semicond. Sci. Technol.* 6, 725 (1991).
56. Z. Zhaochun, P. Ruiwu, and C. Nianyi, *Mater. Sci. Eng. B* 54, 149 (1998).
57. K. Momma and F. Izumi, *J. Appl. Crystallogr.* 44, 1272 (2011).
58. I. Ahmad and M. Maqbool, *Comput. Phys. Commun.* 185, 2829 (2014).
59. C.M.I. Okoye, *J. Phys. Condens. Matter* 15, 5945 (2003).
60. F. Wooten, *Optical Properties of Solids* (New York: Academic, 1972).
61. N. Korozlu, K. Colakoglu, E. Deligoz, and Y.O. Ciftci, *Opt. Commun.* 284, 1863 (2011).
62. B. Amin, I. Ahmad, M. Maqbool, S. Goumri-Said, and R. Ahmad, *J. Appl. Phys.* 109, 023109 (2011).
63. P. Ravindran, A. Delin, B. Johansson, O. Eriksson, and J.M. Wills, *Phys. Rev. B* 59, 1776 (1999).